Scanning Activity Gravimetric Analysis

Adam P. Olsen, Richard C. Flagan,* and Julia A. Kornfield*

Division of Chemistry and Chemical Engineering, California Institute of Technology, Pasadena, California 91125

Received May 8, 2006; Revised Manuscript Received June 19, 2006

ABSTRACT: We introduce a new technique—scanning activity gravimetric analysis (SAGA)—for investigating phase transitions in semicrystalline polymers. Isothermal growth and dissolution of polymer crystallites within picogram to milligram samples are manifested by mass changes in response to changes in the activity of sorbed solvent vapor. Single charged particles are levitated and weighed in an electrostatic field, providing access to highly supersaturated states. Phase transitions are inferred from simultaneous sorption and light scattering measurements. Analogous to differential scanning calorimetry, scanning solvent activity up and down exposes broad transitions between the semicrystalline solid state and the dissolved state, which are influenced by sample history. We demonstrate repeated dissolution and crystallization of an 11 ng sample of poly(ethylene oxide) by controlling the activity of sorbed water vapor and observe self-nucleation of crystallites from partially and fully solvated states.

Introduction

Many polymers crystallize to form chain-folded platelets or ribbons called lamellae that have thickness on the order of 10 nm and may grow beyond a micrometer in length and width.[1] Molecular segments repeatedly traverse the smallest dimension to create two high-energy surfaces of folds and dangling chains that significantly destabilize lamellae relative to the equilibrium extended chain crystal, which is unattainable because of kinetic frustration associated with long entangled molecules. Polymer crystals are thus metastable structures;[2] lamellar thickness is determined not by thermodynamics but by growth kinetics in a supercooled melt or supersaturated solution. Lamellae are separated by amorphous domains, which sequester severe entanglements or defects that are excluded by crystals; polymers, therefore, are typically classified as semicrystalline.

Nucleation processes figure prominently in both early and late stages of polymer crystallization.[1,3,4] Primary nucleation is the formation of a stable volume of ordered material from an amorphous melt or solution; it often occurs heterogeneously in the presence of foreign catalytic surfaces but may also occur homogeneously in samples that are free of impurities. Secondary nucleation, also called molecular nucleation,[5] is the irreversible attachment of one or more stems of an amorphous polymer chain to a growing crystallite. Once anchored, the entire molecule is reversibly incorporated into the crystal. Both nucleation processes proceed at appreciable rates only far from equilibrium, which explains the unique metastability of partially melted polymer samples.[6] Few fundamental measurements of the rates of these important processes have been reported due to the difficulty of making direct observations that are not influenced by foreign surfaces or inclusions.

This paper introduces the application of single particle levitation[7] to the study of semicrystalline polymers. Isolated micron-sized samples of polymer are levitated in an electrostatic field and exposed to solvent vapor at variable partial pressure. As the polymer sorbs and evaporates solvent, and consequently undergoes dissolution and crystallization transitions, sample mass and optical properties are continuously monitored. The large surface-to-volume ratio enables rapid equilibration of heat and mass transport within the sample, thereby minimizing the measurement time. The small volume also minimizes the likelihood that the sample contains foreign inclusions that may serve as heterogeneous nuclei. Levitated samples have surfaces that contact only a gas, in contrast with previous studies of polymer nucleation in which ensembles of dispersed droplets were in contact with foreign condensed matter.[8−12]

A diversity of methods have been used to characterize the kinetics of crystallization in polymers.[13−29] Among these, the most widely implemented is differential scanning calorimetry (DSC), which provides a point of departure for the experimental methods presented below. Kinetics of crystallization are most frequently described in qualitative terms using the rate of heat evolution during cooling at a constant rate. For example, the effect of nucleating agents is often reported in terms of the upward shift of the temperature at which the maximum heat evolution rate occurs during cooling.[22−24] Here we show that analogous information can be obtained under isothermal conditions by decreasing the activity of a solvent.

Calorimetry has also been a powerful tool to probe the melting of lamellae, which typically occurs over a range of temperatures during heating at a constant rate. Coordinated DSC and SAXS (small-angle X-ray scattering) or AFM (atomic force microscopy) measurements have shown that the broad melting transition is largely due to the distribution of lamellar thickness present in the semicrystalline nanostructure; the thinnest lamellae melt at the lowest temperatures in the endotherm, and progressively thicker lamellae contribute to the endotherm as temperature increases.[17,25] Interestingly, heating to temperatures that completely melt all lamellae that can be detected by SAXS or microscopy does not necessarily erase all memory of the previous solid state;[26−31] the microscopic basis of the "melt memory effect" is not yet well understood. Here we show that ramping up the activity of solvent exposes an analogous, broad dissolution isotherm and that, upon reversal of the activity scan after dissolution of the lamellae, memory of the previous solid-state affects the degree of supersaturation that must be reached to trigger regrowth of lamellae.

Scanning activity gravimetric analysis (SAGA) permits protocols analogous to DSC, such as constant scan rate up or

* Corresponding authors. E-mail: flagan@caltech.edu, jak@cheme.caltech.edu.

10.1021/ma061027r CCC: $33.50
Published on Web 07/22/2006

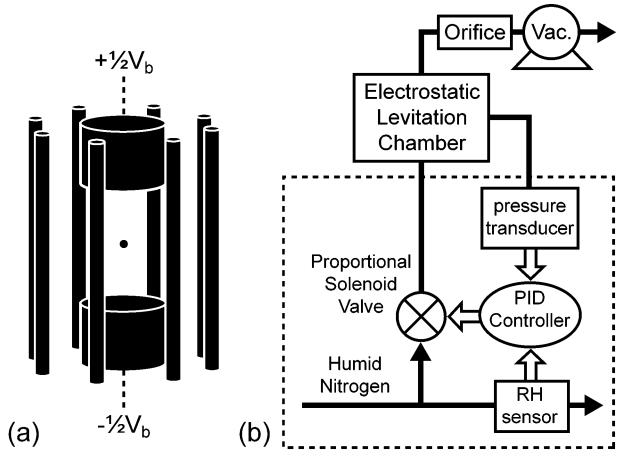

Figure 1. (a) Schematic of electrode cage for electrostatic levitation showing particle balanced at the geometric center. (b) Schematic of the environmental control module. The activity of water at the particle is controlled by modulating the pressure of a nitrogen stream containing a fixed mole fraction of water vapor. The levitation chamber, humidifier, and relative humidity (RH) sensor are held at constant temperature with recirculating fluid.

down in activity or discrete jumps up or down in activity. Analogous to DSC measuring heat flux to a sample in response to changing temperature, SAGA monitors the absorption or evaporation of solvent in response to changing activity. The present work investigates crystal nucleation, growth, and dissolution in aqueous poly(ethylene oxide) (PEO) under isothermal conditions.

Experimental Section

An automated single particle electrostatic levitation system, described in detail elsewhere,[32] was used to perform SAGA on PEO (Sigma Aldrich Co.; M_w = 100 000 g/mol), scanning the activity of water. A three-dimensional electrostatic field generated by a cage of electrodes (Figure 1a) suspends a micron-sized charged particle against gravitational, aerodynamic, and Brownian forces; the DC balancing voltage (V_b) applied across the disk electrodes shown in Figure 1a is proportional to mass. Automated position control maintains the particle within a finite view volume defined by an illuminating laser beam as the sorbed water content equilibrates with the humid atmosphere. The balancing voltage is continuously recorded during an experiment, and relative mass (m/m_0) is calculated by normalizing the instantaneous balancing voltage by the balancing voltage in the dry state, i.e., $m/m_0 = V_b/V_{b,dry}$.

The relative humidity (water activity, a_w) and temperature of a nitrogen atmosphere surrounding the particle are strictly regulated by an environmental control module (Figure 1b). The apparatus can be programmed to impose any desired water activity history; the experiments described below use simple constant rate scans. The humidity in the sample chamber equals that of the inlet stream at low to moderate water activity ($a_w < 0.80$). At high water activity ($a_w > 0.80$), the humidity at the sample slightly lags that of the inlet stream. A calibration procedure is implemented to correct for the instrument lag, as described in the Supporting Information.

Dissolution and crystallization are directly observed through changes in water content and optical properties. When all crystallites dissolve, the sample becomes a spherical droplet of polymer solution. A micron-sized optically homogeneous sphere, such as a small solution droplet, produces a well-defined angular scattering pattern, known as Mie scattering,[33] when illuminated by coherent light. The Mie pattern exhibits a series of peaks and valleys in scattered intensity with an angular frequency that increases with diameter. Thus, the observed light scattering pattern (Figure 2) provides a measure of the absolute size of the solution droplet. In contrast, an aspherical particle or one with internal heterogeneity produces an irregular light scattering pattern. Therefore, the Mie pattern is lost upon formation of a crystallite in a droplet of supersaturated solution.

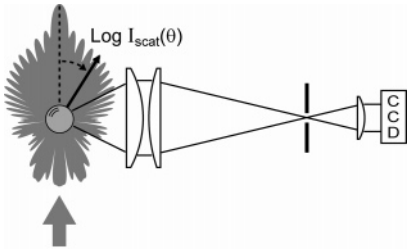

Figure 2. Optical configuration for collection of angular light scattering between 78° and 102° relative to the incident laser beam (532 nm, 25 mW). Radiation is focused through an aperture and collimated onto a CCD detector. A logarithmic polar plot of the calculated scattered light intensity as a function of angle for a 5 μm droplet is superimposed.

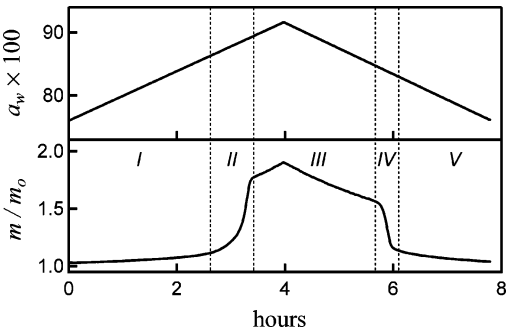

Figure 3. Response of the PEO particle to a continuous triangular scan in water activity between 0.76 and 0.92 at 0.04 h^{-1}. Particle mass is normalized by the mass of the dry particle. T = 21.10 ± 0.05 °C.

All gravimetric data presented below were recorded during a series of experiments using a single 11 ng particle of PEO, corresponding to a dry diameter of ~26 μm. The results accord well with measurements made on a number of other particles of the same PEO.

Results

Poly(ethylene oxide) (PEO) exhibits an asymmetric response to humidification as the activity of water within a levitated particle increases and decreases between 0.76 and 0.92 with a scan rate of 0.04 h^{-1} (Figure 3). Starting from a nearly dry solid state, as a_w increases, the particle mass increases slightly by sorption of water into the semicrystalline structure[34−36] (zone I, Figure 3). As a_w increases further, however, it eventually becomes large enough that the water content increases strongly (zone II, Figure 3) as polymer crystallites dissolve, eventually yielding an aqueous solution droplet (zone III, Figure 3).

The transition from the semicrystalline solid with sorbed water to the dissolved aqueous solution droplet is termed deliquescence. Deliquescence of hygroscopic aerosols governs the formation of liquid droplets in the atmosphere and has been extensively studied for its influence on global climate.[37−39] A substance with a well-defined crystal structure, such as a pure inorganic salt, exhibits a simple response to humidification. A sodium chloride particle, for example, absorbs no water with increasing a_w up to the deliquescence point ($a_{w,d}$). The particle then spontaneously dissolves over an extremely narrow range of activity to generate an aqueous solution droplet; salt deliquescence appears graphically as a sharp vertical transition. The PEO particle, in contrast, displays finite water absorption even at low activity, and deliquescence occurs over a relatively wide activity range. This behavior is analogous to that of mixed salt particles, which deliquesce stepwise over a range in activity as the various components activate sequentially.[40] Semicrystal-

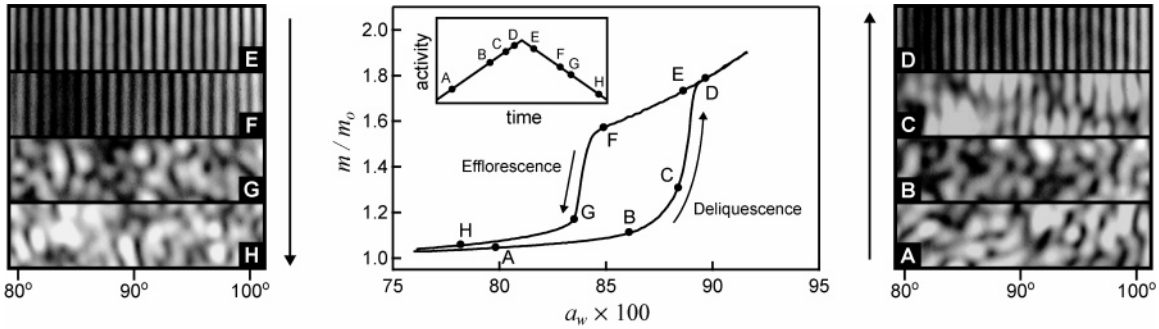

Figure 4. Parametric plot (m/m_0 vs a_w) of thermodynamic data in Figure 3 and images of angular light scattering collected at various times (A−H).

line polymer may contain a population of crystallites with varying thickness. Since the free energy of a polymer crystal is a function of lamellar thickness, the thinnest lamellae will dissolve at lower water activity than thicker lamellae. Variable stability in polymer samples with uniform lamellar thickness has also been reported and has been attributed to interactions between neighboring lamellae.[41]

At water activity above the deliquescence transition ($a_w > a_{w,d}$), the solution continuously sorbs or evaporates water as a_w increases or decreases along the vapor−liquid isotherm (zone III, Figure 3). Indeed, after dissolving the crystallites, it is possible to continue along the vapor−liquid isotherm into the supersaturated regime by reducing a_w below $a_{w,d}$: hence, the asymmetry in the sorption behavior. During the downward scan, zone III continues until the solution becomes sufficiently supersaturated that nucleation occurs on the time scale of the experiment. Propagation of crystallites throughout the particle then drives evaporation of water in a process known as efflorescence (zone IV, Figure 3).

Efflorescence, unlike deliquescence, may occur far from equilibrium and is, therefore, ideally probed with single particle techniques. Particle levitation eliminates container surfaces that might catalyze nucleation and enables isolation of microscopic sample volumes in which highly supersaturated states can be probed; the activity at which a system effloresces ($a_{w,e}$) depends on sample size and purity. Again, it is useful to compare the efflorescence observed in the polymer solution to that in a simple salt. For example, decreasing a_w to $a_{w,e}$ in a small drop of supersaturated NaCl solution produces complete expulsion of water over a very narrow range of a_w: as soon as a nucleation event occurs, crystal growth rapidly (in effect, instantaneously) incorporates all of the salt. In contrast, PEO crystallization proceeded over a substantial interval of a_w, leading to the finite slope in zone IV (Figure 3). The PEO particle also retained residual water after the steep decrease in mass; continued reduction in a_w led to further decrease in the mass (zone V) as it gradually approached that of the solid during the up scan (zone I). This "tail" at low activity reflects the slow evolution of crystal morphology characteristic of semicrystalline polymers (e.g., due to secondary crystallization processes).[1,16−18]

A parametric plot of the recorded mass and water activity clearly illustrates hysteresis between increasing and decreasing scans (Figure 4). Representative light scattering patterns confirm the correlation between the sorption/desorption behavior and the dissolution/formation of crystallites (Figure 4, A−H). The uniform vertical Mie fringes in images D, E, and F indicate a spherical, optically homogeneous droplet. Images A, B, G, and H each display irregular scattering, a signature of optical heterogeneities and/or deviations from spherical shape. Image C, of the partially dissolved state, displays distorted Mie fringes indicative of a droplet with only minor surface roughness or

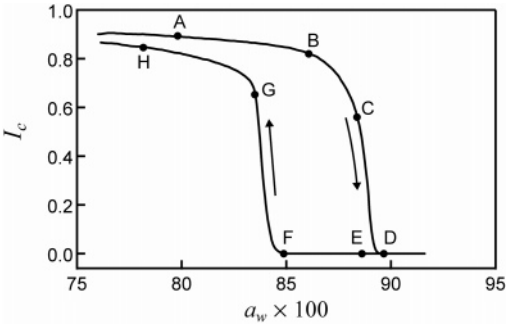

Figure 5. I_c vs a_w for the data in Figures 3 and 4.

internal heterogeneity. Comparison of the fringe spacing in image D ($m/m_0 = 1.8$) with Mie theory (assuming refractive index 1.40) indicates a droplet diameter of 33 ± 1 μm, corresponding to a dry PEO mass of 11 ± 1 ng. The analysis is weakly dependent on the choice of refractive index; e.g., using either the refractive index of pure water or amorphous PEO yields a result within the stated uncertainty.

The presence of crystallites correlates with a negative deviation from the solution isotherm. The most extreme possible decrease in mass corresponds to complete expulsion of water, i.e., dropping to m_0. Therefore, an index that increases from 0 to 1 as crystallinity increases may be constructed and applied to the data discussed above (Figure 5):

$$I_c(a_w) = \frac{m_{sol}(a_w) - m(a_w)}{m_{sol}(a_w) - m_0} \quad (1)$$

where m_0 is the mass of the dry PEO particle, $m(a_w)$ is the actual mass of the PEO particle at a given water activity, and $m_{sol}(a_w)$ is the equilibrium mass of the fully dissolved PEO solution droplet at a given water activity; $m_{sol}(a_w)$ is obtained from the final experiment presented below. The water content of the PEO particle depends on the crystal morphology and the hygroscopicity of the various crystalline and noncrystalline domains. The index I_c is a measure of the average hygroscopicity of the particle, normalized by that of the fully dissolved state ($I_c \equiv 0$ on the solution isotherm). PEO crystallinity has been reported to be as high as 85% when measured by calorimetry;[42] although the present index is not expected to correspond precisely to the volume fraction of material that is crystalline, we observe that I_c increases to ~90% at the greatest level of crystallinity in our experiments.

The hysteresis in sorption persists even if a substantial population of crystals is deliberately left in the sample at the peak of the scan in a_w (Figure 6). The PEO particle was partially dissolved by increasing a_w only to selected values during scans B ($a_w = 0.892$) and C ($a_w = 0.894$) before drying. Prior to each of scans B and C, the particle was brought to the solution

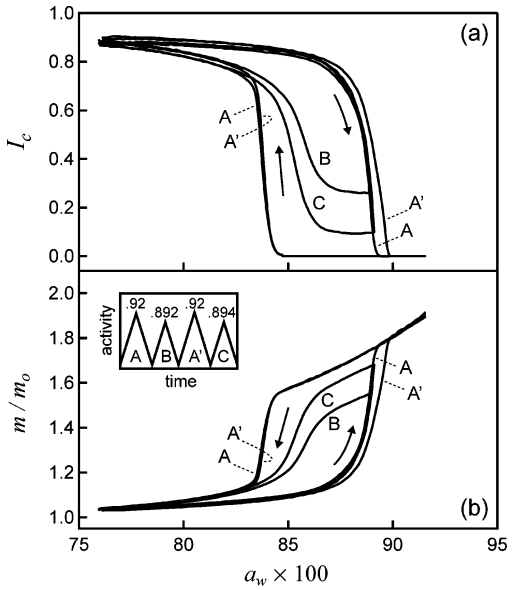

Figure 6. (a) I_c vs a_w and (b) m/m_0 vs a_w for four consecutive triangular scans in a_w (inset) at 0.04 h^{-1}. $T = 21.10 \pm 0.05$ °C. In each case the activity scan begins at 0.76. To create similar solid state structures for scans B and C, the scans A and A′ take the specimen up to $a_w = 0.92$ (beyond complete deliquescence). Scans B and C have peak values 0.892 and 0.894, respectively.

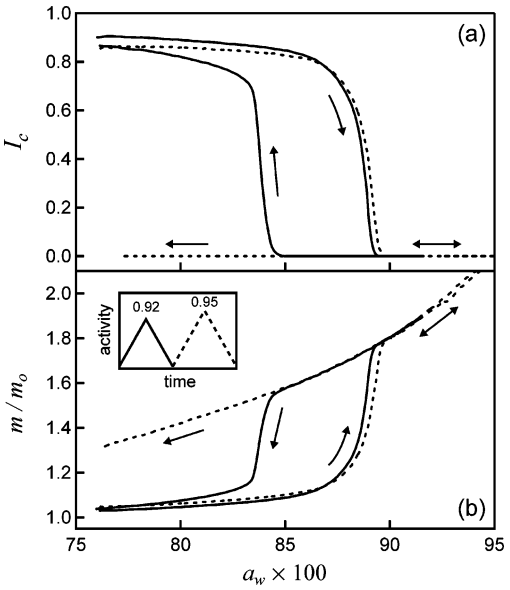

Figure 7. (a) I_c vs a_w and (b) m/m_0 vs a_w for two consecutive triangular scans in a_w between 0.76 and 0.92 (solid) and 0.95 (dashed) at 0.04 h^{-1}. $T = 21.10 \pm 0.05$ °C.

state and then recrystallized with an annealing scan that peaked at $a_w = 0.92$ (scans A and A′). The importance of annealing is demonstrated by the deviation of A′ from A during deliquescence; the upward shift in $a_{w,d}$ indicates that scan B caused a shift in the population of lamellae toward more stable crystallites. The deliquescence response during scans B and C, however, agrees well, indicating similar initial solid-state morphologies, since scans A and A′ exhibited identical values of $a_{w.e}$. One unfamiliar with semicrystalline polymers might expect that the residual crystalline material would grow immediately upon drying during scans B and C. When the activity in the partially solvated particle was decreased, however, I_c remained roughly constant for a time before the particle effloresced, albeit at higher $a_{w,e}$ than for the fully solvated droplets of scans A and A′. The hysteresis indicates that the rate of secondary nucleation, which is required for crystal growth, is negligible at $a_{w,d}$ but increases with decreasing a_w. That $a_{w,e}$ increased clearly indicates that efflorescence was not initiated by homogeneous nucleation; instead, the residual crystalline material catalyzed a form of heterogeneous nucleation known as self-nucleation at sufficiently low activity.

The nature of the efflorescence transition in scans A and A′ (Figure 6) can be revealed by increasing the peak a_w to even higher values. The environmental control module was programmed to ramp the activity of water up and down between $a_w = 0.76$ and 0.95 (dashed curve in Figure 7) at a scan rate of 0.04 h^{-1} immediately following a scan up to $a_w = 0.92$ (solid curve in Figure 7). As a_w decreased from 0.95, the solution droplet remained metastable well below the activity at which crystallization occurred in the previous scans. During numerous related "annealing" experiments with other particles than the one used in the present experiments, efflorescence relative humidity varied between $a_{w,e} = 0$ (dry nitrogen) and 0.85 depending on the precise sample history.[43]

Discussion

Physics of Polymer Deliquescence. Sorption into solid-state semicrystalline polymers has been extensively investigated.[34−36] It is well established that at low levels of sorption the solvent penetrates the interlamellar−noncrystalline material, but not the crystallites themselves. To our knowledge, however, deliquescence of polymers has not been reported previously. Consequently, the opportunity to characterize lamellar stability distributions under isothermal conditions using deliquescence was not recognized.

The deliquescence behavior truly probes the instantaneous distribution of crystallite stabilities and is not limited by kinetics of solvent penetration through the droplet. When the scan rate in increased by a factor of 8 (from 0.04 to 0.32 h^{-1}), the deliquescence behavior is unaffected. Therefore, the scan rate used here is sufficiently slow that the activity of the solvent is uniform throughout the sample and equal to that imposed by the surrounding vapor.

As the solvent activity is increased, a transition occurs from sorption into a composite in which the crystallites remain intact to sorption accompanied by selective dissolution of those crystallites that, by virtue of their thickness or the nature of the adjacent noncrystalline material, or both, are not stable at the instantaneous activity. We have shown that there is a drastic separation in time scales between this selective dissolution process and the subsequent remodeling of the lamellar distribution to form more stable crystallites (on a time scale of ∼10 h when held at constant activity).[43] Therefore, the present continuous scans reflect the selective dissolution only.

Dissolution of the least stable lamellae affects sorption in two ways. First, it can open a wide, noncrystalline layer sandwiched by two surviving lamellae that remain connected by tie chains and interlocked loops. In this region the constraints on the noncrystalline strands are greatly reduced, and sorption may proceed to a greater extent than in the noncrystalline regions that were tightly constrained prior to the dissolution of the intervening lamella. Second, dissolution of lamellae will result in some polymer chains becoming completely untethered from any crystallite. These chains are free to diffuse to pockets of polymer solution that coexist with swollen semicrystalline domains. Since the activity of water is uniform throughout the sample, these pockets of solution have a water:polymer ratio given by that of the equilibrium solution−vapor isotherm.

Interpretation of I_c. The index I_c defined by eq 1 has been constructed to deconvolute differences in sorbed solvent content caused by changes in crystal morphology from those caused by changes in solvent activity. It provides a means of making relative comparisons of the degree of crystallinity of a sample at different solvent activities, although we do not recommend that it be used as a quantitative measure. If we could assume that crystalline domains within the semicrystalline structure are impermeable to solvent and that noncrystalline domains sorb solvent to the same extent as the fully dissolved polymer, only then would I_c indicate the volume fraction of crystalline material. The assumption regarding the crystalline domains is substantiated.[34] Because of constraints imposed by the cross-linked network of lamellae, however, noncrystalline material in the interlamellar space is expected to sorb less solvent than dissolved polymer at a given activity. The index I_c, therefore, is always greater than the volume fraction of crystalline material. The nonideality, and thus the discrepancy between I_c and X_c, vanishes as I_c approaches 0.

History Effects on Polymer Efflorescence. In contrast to the absence of kinetic effects during deliquescence, strong effects of scan rate and sample history are seen during efflorescence. A small change in the maximum water activity (e.g., from 0.92 to 0.95 in Figure 7) can transform the behavior from a distinct efflorescence event at a moderate supersaturation ($a_{w,e} = 0.84$) to requiring a supersaturation beyond the range probed in the experiment (i.e., $a_{w,e} < 0.76$). Since the latter provides a bound on homogeneous nucleation, it is clear that nucleation in the former was heterogeneous even though the polymer appeared to be fully solvated after a peak activity of $a_w = 0.92$. Since the heterogeneous nuclei can be erased by a modest change in history, they are not due to contaminant particles. The efflorescence observed in scans A and A′ (Figure 6) and also in Figure 4, therefore, must have been initiated by remnants of lamellae[26−29] that remained after scanning to $a_w = 0.92$; these remnants appear to have been erased, however, during a scan up to $a_w = 0.95$.

SAGA: A Powerful Probe of Thermodynamic and Kinetic Aspects of Polymer Crystallization. To illustrate the capabilities of SAGA, we begin with analogies to DSC that show how SAGA experiments can be designed and interpreted on the basis of familiar protocols used to study crystallization and melting using calorimetry. We close by highlighting unique experiments that are enabled by SAGA, which are not possible within the limitations of calorimetry.

Those familiar with DSC will immediately recognize that the deliquescence and efflorescence activities ($a_{w,d}$ and $a_{w,e}$) identified by SAGA are analogous to the melting and crystallization temperatures (T_m and T_c) of DSC. Each technique observes that phase transitions proceed over a wide range during linear scans in activity or temperature, and each also permits other protocols such as discrete jumps. DSC typically assigns the nominal temperature of a transition to that which exhibits the maximum heat flux. The analogous assignment of nominal activity in our experiments would be that which exhibits the maximum rate of water sorption or evaporation, corresponding to the inflection points in zones II and IV (Figure 3). It should be noted that the heat flux that is monitored by DSC is analogous to the derivative of the mass of sorbed solvent that is monitored by SAGA.

History effects that figure prominently in semicrystalline polymers can be probed by SAGA with protocols reminiscent of those used in calorimetry. Semicrystalline material continuously evolves after primary crystallization to maximize the degree of crystallinity and minimize high-energy fold surfaces. These secondary crystallization processes include thickening of existing lamellae and nucleation and growth of thin platelets in the interlamellar space. DSC detects the consequences of these sluggish processes through changes in the melting behavior after well-defined annealing protocols.[17,18] Likewise, SAGA can discriminate changes in sorption behavior that may result from changes in crystal morphology (e.g., the distribution of lamellar thickness) through shifts in $a_{w,d}$ (cf. scans A and A′, Figure 6). Since sorption tracks the transient hygroscopicity, related to the crystalline content, SAGA can readily track gradual evolution of crystallinity over very long times (zone V, Figure 3) that are inaccessible by conventional DSC, which requires relatively rapid changes in crystallinity to generate a measurable heat flow.

Another fascinating history dependence observed in semicrystalline polymers is the "melt memory effect": even when heated beyond the apparent melting transition, the prior semicrystalline state can influence subsequent crystallization upon cooling. Although the mechanism is not known, the "memory" may arise from small remnants of lamellae that persist above the nominal melting point[26−28] and then serve as athermal nuclei[44] upon cooling. In calorimetry, the effect is manifested after a thermal quench as a shift in the time τ at which the maximum isothermal crystallization rate is observed. Relative to annealing above the equilibrium melting temperature, τ increases by an amount that is a function of annealing time and temperature.[29] SAGA displays an analogous "memory effect": scanning to $a_w = 0.95$ enabled the PEO solution droplet to achieve much greater supersaturation upon drying than did a scan to $a_w = 0.92$ (Figure 7). In a forthcoming paper we will demonstrate a reversal of this the trend, causing $a_{w,e}$ to systematically increase, by careful selection of a scanning activity protocol.[43]

SAGA is ideally suited for investigating nucleation kinetics since a single material specimen can be repeatedly probed for statistical analysis.[32,45−47] Elimination of container surfaces that might catalyze nucleation and isolation of microscopic sample volumes allow access to highly supersaturated states. Electrostatic levitation has been successfully implemented with sample mass ranging from less than a picogram[48] ($D_p < 1\ \mu$m) to greater than a milligram[49] ($D_p > 1$ mm), although not with identical instruments. Since only a single nucleation event is required to crystallize an entire sample, SAGA thus has the potential to probe at least 9 orders of magnitude in nucleation rate (i.e., events per unit volume per unit time) with experiments performed on similar time scales; extending measurement times will further enhance the dynamic range.

The most obvious departure from DSC is that SAGA directly controls the chemical potential under isothermal conditions. Polymer crystallization and dissolution proceed without simultaneous changes in the enthalpy of fusion that accompany studies of polymer crystallization from the melt or traditional studies of polymer crystallization from solution, which control the temperature at fixed (and usually very dilute) concentration.[50] The small surface-to-volume ratio of levitated particles facilitates uniform changes in the concentration of sorbed solvent that would take prohibitive time to equilibrate in bulk samples. Thus, SAGA makes it feasible to explore the free energy landscape at fixed temperature.

Acknowledgment. The authors thank Professor Chris Sorenson and Matthew Berg of Kansas State University, Professor Zhen-Gang Wang of California Institute of Technology, and Professor Nitash Balsara of University of California—Berkeley for insightful discussions. This work was funded by the National

Science Foundation (DMR-0505393 and the MRSEC Program under Award DMR-0080065).

Supporting Information Available: Instrument calibration at high a_w with levitated aqueous sodium chloride droplet. This material is available free of charge via the Internet at http://pubs.acs.org.

References and Notes

(1) Strobl, G. R. *The Physics of Polymer: Concepts for Understanding Their Structures and Behavior*; Springer-Verlag: Berlin, 1996.
(2) Cheng, S. Z. D.; Keller, A. *Annu. Rev. Mater. Sci.* **1998**, *28*, 533−562.
(3) Hoffman, J. D.; Davis, G. T.; Lauitzen, J. I., Jr. The rate of crystallization of linear polymers with chain folding. In *Treatise on Solid State Chemistry*; Hannay, N. B., Ed.; Plenum: New York, 1976; Vol. 3, Chapter 7, pp 497−614.
(4) Cheng, S. Z. D.; Lotz, B. *Polymer* **2005**, *46*, 8662−8681.
(5) Wunderlich, B.; Mehta, A. *J. Polym. Sci., Part B* **1974**, *2*, 255−263.
(6) Banks, W.; Gordon, M.; Sharples, A. *Polymer* **1963**, *4*, 289−302.
(7) Davis, E. J. *Aerosol Sci. Technol.* **1997**, *26*, 212−254.
(8) Cormia, R. L.; Price, F. P.; Turnbull, D. *J. Chem. Phys.* **1962**, *37*, 1333−1340.
(9) Koutsky, J. A.; Walton, A. G.; Baer, E. *J. Appl. Phys.* **1967**, *38*, 1832−1839.
(10) Arnal, M. L.; Matos, M. E.; Morales, R. A.; Santana, O. O.; Müller, A. J. *Macromol. Chem. Phys.* **1998**, *199*, 2275−2288.
(11) Loo, Y.-L.; Register, R. A.; Ryan, A. J. *Phys. Rev. Lett.* **2000**, *84*, 4120−4123.
(12) Massa, M. V.; Carvalho, J. L.; Dalnoki-Veress, K. *Eur. Phys. J. E* **2003**, *12*, 111−117.
(13) Alfonso, G. C.; Russell, T. P. *Macromolecules* **1986**, *19*, 1143−1152.
(14) Fillon, B.; Wittman, J. C.; Lotz, B.; Thierry, A. *J. Polym. Sci.* **1993**, *31*, 1383−1393.
(15) Okazaki, I.; Wunderlich, B. *Macromolecules* **1997**, *30*, 1758−1764.
(16) Wang, Z.-G.; Hsiao, B. S.; Sauer, B. B.; Kampert, W. G. *Polymer* **1999**, *40*, 4615−4627.
(17) Alizadeh, A.; Richardson, L.; Xu, L.; McCartney, S.; Marand, H.; Cheung, Y. W.; Chum, S. *Macromolecules* **1999**, *32*, 6221−6235.
(18) Marand, H.; Huang, Z. *Macromolecules* **2004**, *37*, 6492−6497.
(19) Imai, M.; Mori, K.; Mizukami, T.; Kanaya, T. *Polymer* **1992**, *33*, 4451−4456.
(20) Terrill, N. J.; Fairclough, P. A.; Towns-Andrews, E.; Komanschek, B. U.; Young, R. J.; Ryan, A. J. *Polymer* **1998**, *39*, 2381−2385.
(21) Kumaraswamy, G.; Issaian, A. M.; Kornfield, J. A. *Macromolecules* **1999**, *32*, 7537−7547.
(22) Fillon, B.; Thierry, A.; Lotz, B.; Wittman, J. C. *J. Therm. Anal.* **1994**, *42*, 721−731.
(23) Bauer, T.; Thomann, R.; Mülhaupt, R. *Macromolecules* **1998**, *31*, 7651−7658.
(24) Nagarajan, K.; Levon, K.; Myerson, A. S. *J. Therm. Anal. Calorim.* **2000**, *59*, 497−508.
(25) Krüger, K. N.; Zachmann, H. G. *Macromolecules* **1993**, *26*, 5202−5208.
(26) Janeschitz-Kriegl, H. *Colloid Polym. Sci.* **1997**, *275*, 1121−1135.
(27) Janeschitz-Kriegl, H.; Ratajski, E.; Wippel, H. *Colloid Polym. Sci.* **1999**, *277*, 217−226.
(28) Janeschitz-Kriegl, H. *Colloid Polym. Sci.* **2003**, *281*, 1157−1171.
(29) Alfonso, G. C.; Ziabicki, A. *Colloid Polym. Sci.* **1995**, *273*, 317−323.
(30) Häfele, A.; Heck, B.; Hippler, T.; Kawai, T.; Kohn, P.; Strobl, G. *Eur. Phys. J. E* **2005**, *16*, 217−224.
(31) Massa, M. V.; Lee, M. S. M.; Dalnoki-Veress, K. *J. Polym. Sci., Part B* **2005**, *43*, 3438−3443.
(32) Olsen, A. P.; Flagan, R. C.; Kornfield, J. A. *Rev. Sci. Instrum.* **2006**, *77*, 073901.
(33) van de Hulst, H. C. *Light Scattering by Small Particles*; Wiley: New York, 1957.
(34) Murthy, N. S.; Akkapeddi, M. K.; Orts, W. J. *Macromolecules* **1998**, *31*, 142−152.
(35) Adriaensens, P.; Pollaris, A.; Carleer, R.; Vanderzande, D.; Gelan, J.; Litvinov, V. M.; Tijssen, J. *Polymer* **2001**, *42*, 7943−7952.
(36) Vergelati, C.; Imberty, A.; Perez, S. *Macromolecules* **1993**, *26*, 4420−4425.
(37) Richardson, C. B.; Spann, J. F. *J. Aerosol Sci.* **1984**, *15*, 563−571.
(38) Tang, I. N.; Munkelwitz, H. R. *J. Colloid Interface Sci.* **1984**, *98*, 430−438.
(39) Cohen, M. D.; Flagan, R. C.; Seinfeld, J. H. *J. Phys. Chem.* **1987**, *91*, 4563−4574.
(40) Tang, I. N.; Munkelwitz, H. R.; Davis, J. G. *J. Aerosol Sci.* **1978**, *9*, 505−511.
(41) Strobl, G. *Prog. Polym. Sci.* **2006**, *31*, 398−442.
(42) Yang, L. B.; Venkatesh, G.; Fassihi, R. *J. Pharm. Sci.* **1996**, *85*, 1085−1090.
(43) Olsen, A. P.; Flagan, R. C.; Kornfield, J. A., submitted.
(44) Fischer, J. C.; Hollman, J. H.; Turnbull, D. *J. Appl. Phys.* **1948**, *19*, 775−784.
(45) Knezic, D.; Zaccaro, J.; Myerson, A. S. *J. Phys. Chem. B* **2004**, *108*, 10672−10677.
(46) Hamza, M. A.; Berge, B.; Mikosch, W.; Rühl, E. *Phys. Chem. Chem. Phys.* **2004**, *6*, 3484−3489.
(47) Krämer, B.; Hübner, O.; Vortisch, H.; Wöste, L.; Leisner, T.; Schwell, M.; Rühl, E.; Baumgärtel, H. *J. Chem. Phys.* **1999**, *111*, 6521−6527.
(48) Schlemmer, S.; Illemann, J.; Wellert, S.; Gerlich, D. *J. Appl. Phys.* **2001**, *90*, 5410−5418.
(49) Rhim, W. K.; Chung, S. K.; Barber, D.; Man, K. F.; Gutt, G. Rulison, A.; Spjut, R. E. *Rev. Sci. Instrum.* **1993**, *64*, 2961−2970.
(50) Blundell, D. J.; Keller, A.; Kovacs, A. J. *J. Polym. Sci., Part B: Polym. Lett.* **1966**, *4*, 481−486.

MA061027R